Lattice Boltzmann equation calculation of internal, pressure-driven turbulent flow

2002 J. Phys. A: Math. Gen. 35 9945

(http://iopscience.iop.org/0305-4470/35/47/301)

INSTITUTE OF PHYSICS PUBLISHING JOURNAL OF PHYSICS A: MATHEMATICAL AND GENERAL

J. Phys. A: Math. Gen. **35** (2002) 9945–9955 PII: S0305-4470(02)39415-0

Lattice Boltzmann equation calculation of internal, pressure-driven turbulent flow

L A Hammond, I Halliday, C M Care and A Stevens

Materials Research Institute, Sheffield Hallam University, Howard Street, Sheffield, S1 1WB, UK

Received 10 July 2002, in final form 2 October 2002
Published 12 November 2002
Online at stacks.iop.org/JPhysA/35/9945

Abstract

We describe a mixing-length extension of the lattice Boltzmann approach to the simulation of an incompressible liquid in turbulent flow. The method uses a simple, adaptable, closure algorithm to bound the lattice Boltzmann fluid incorporating a *law-of-the-wall*. The test application, of an internal, pressure-driven and smooth duct flow, recovers correct velocity profiles for Reynolds number to 1.25×10^5. In addition, the Reynolds number dependence of the friction factor in the smooth-wall branch of the Moody chart is correctly recovered. The method promises a straightforward extension to other curves of the Moody chart and to cylindrical pipe flow.

PACS numbers: 05.50.+q, 15.70.−a, 47.27.−i

1. Introduction

Over the past decade, a range of lattice Boltzmann (LB) methods have been developed as mesoscopic models of isotropic [12] and (very recently) anisotropic [1] fluids. In fact, the LB method shows particular promise when applied to complex situations at low Reynolds number: typically multi-component systems [13, 15] and flows in complex geometry [8]. However, the LB method is not confined to these applications and the past few years have seen a growing level of interest in applying LB in areas where more conventional computational fluid dynamics (CFD) is well established. One such area is that of incompressible, internal turbulent flow.

Turbulent flow has been addressed with LB most thoroughly in the context of external flows. Here, it might be argued that the leading edge of the technology lies outside academia and with companies such as the Exa Corporation [2]; as a consequence, LB should certainly not be viewed as an immature technology. Recent papers in this area treat demanding problems (e.g., an axial compressor cascade [3]) with considerable sophistication. Multi-scale LB schemes and a k–ϵ turbulence model [3] have also been developed. See also the references cited in chapter 9 of [12]. In the present paper we consider internal flow.

In applications, turbulent pipe flow is more important than duct flow, but more difficult to implement. However, for the purposes of turbulence modelling, the two cases possess many common features [16], making the latter an appropriate and accessible test-bench. Accordingly, in this paper, we propose and validate a turbulent LB scheme for an infinite aspect ratio duct. The method may be subsequently extended to the simulation of cylindrical pipe flow.

Setting aside as impractical, the direct simulation of turbulent length scales, one has a wide choice of strategies from which to choose. The k–ϵ and the Prandtl *mixing-length* models are but two, albeit popular, approaches [16]. Both recover, from the solution of appropriately modified (Reynolds-averaged) Navier–Stokes equations, what are essentially time-averaged velocity fields, in which the *sub-grid scale* turbulence has been averaged [16]. In both cases, the accepted device of a turbulent contribution to the molecular viscosity is central.

The dynamics of an LB fluid is expressed through the form of the continuity and momentum (Navier–Stokes) equations, recovered from its particular microscopic evolution algorithm. Here, when discussing our approach in section 2, we attempt carefully to highlight how the 'mixing-length' modification, to the basic LB algorithm of Teixeira [14], actually modifies the lattice fluid. The changes are measured by the precise form of its Navier–Stokes and continuity equations and as such are exactly to account for the (time-averaged) influence of turbulence through additional modelled stresses. This precisely follows the traditional method of Reynolds-averaged stresses, a point to which we shall return.

Accurate representation of a boundary is as central in LB as in any other branch of CFD and this is especially true for turbulent flows. Our chosen closure strategy [5], applied in section 3 is demonstrably second-order accurate. We adapt the method to represent the slip velocity at the outer (wet) side of the viscous sub-layer, which occurs close to the wall in turbulent duct flow. Accordingly, in the discussions of section 3, lattice boundary nodes lie *within* the lattice fluid at the appropriate distance.

In section 4, we present results of turbulent, smooth-duct flow and consider the form of the velocity profile that results when turbulent flow is forced by a uniform pressure gradient, as is implemented through a uniformly impressed body force. More importantly, we also consider the variation of the Darcy–Weisbach friction factor over a large range of Reynolds number, to recover excellent agreement with experiment. In section 5, we present our conclusions and proposals for future work.

2. Preliminary analysis

To describe the flow of an incompressible, turbulent fluid, workers most often calculate a velocity field which has been averaged over a time scale long relative to the turbulence. It can be shown that this velocity field, conventionally denoted by U_α, is governed by the usual continuity equation, together with momentum (Navier–Stokes) equations modified to include the influence of the turbulence through the *Reynolds stresses*, $\tau_{\alpha\beta}$ [16]

$$\partial_t \rho U_\alpha + U_\beta \partial_\beta \rho U_\alpha = -\partial_\alpha P + \partial_\beta (\nu_0 \rho S_{\alpha\beta}) + \partial_\beta \tau_{\alpha\beta} \tag{1}$$

where $S_{\alpha\beta}$ is the strain rate tensor based on U. The Prandtl mixing-length approach to modelling turbulence entails the physical assumption:

$$\tau_{\alpha\beta} = \nu_t \rho S_{\alpha\beta} \tag{2}$$

which, when substituted into equation (1), generates an additive 'correction' to the usual *molecular* kinematic viscosity ν_0 in the turbulent fluid's effective stress tensor [16]

(see below). The *turbulent* viscosity ν_t appearing in equation (2) is position dependent and is given, after Prandtl, by

$$\nu_t = l_{\text{mix}}^2 |S_{\alpha\beta}| \tag{3}$$

where all symbols have their usual meaning; $|S_{\alpha\beta}| = (S_{\alpha\beta} S_{\alpha\beta})^{1/2}$ and l_{mix} is the *mixing length*, an empirical parameter which generally varies with position in the flow domain. In fact, the mixing length is intended to register the scale of turbulent eddies from physical considerations, usually the placement of solid boundaries. Accordingly, a mixing-length field is generally input into particular flow calculations, often from practical experience and physical intuition. In the particular case of uniform duct flow, with infinite aspect ratio and translational invariance in the x-direction, it is common in traditional CFD to assume a *fourth-power model* across the y-direction [16]:

$$l_{\text{mix}} = \frac{W}{2}\left[0.14 - 0.08\left(1 - \frac{y}{W/2}\right)^2 - 0.06\left(1 - \frac{y}{W/2}\right)^4\right] \tag{4}$$

in which the parameter W is the width of the duct and a value of 0.41 for the von Kármán constant is implicit. Thus, a modified *effective* viscosity

$$\nu = \nu_0 + \nu_t \tag{5}$$

replaces the molecular viscosity in the viscous stress term of the Navier–Stokes equations describing the fluid, giving

$$\partial_t \rho U_\alpha + U_\beta \partial_\beta \rho U_\alpha = -\partial_\alpha P + \partial_\beta((\nu_0 + \nu_t)\rho S_{\alpha\beta}). \tag{6}$$

Equation (6) is solved for time-averaged velocity and pressure fields after imposing appropriate velocity boundary conditions and combining with the continuity equation. Again, we emphasize that the governing equations now yield quantities time-averaged relative to *sub-grid* turbulent fluctuations. They assume a more complicated character, as the viscosity acquires a spatial dependence through $S_{\alpha\beta}$, which appears in ν_t. Moreover, with the effective viscosity now a combination of molecular and turbulent components, it ceases to characterize the fluid alone and must be regarded as characteristic of the overall problem: geometry, fluid and Reynolds number.

In LB hydrodynamics, the simulated fluid's viscosity ν is determined by the algorithm's collision parameter τ, the notation for which should cause no confusion with the Reynolds stress tensor $\tau_{\alpha\beta}$. Thus, to embed the mixing-length model into an LB scheme, one might use the device of inserting the target spatial dependence directly into the collision parameter, τ, in such a way as to recover the form for the viscosity given by equation (5). We now consider the consequences of spatial dependence in τ, by following the analysis carefully through to the lattice fluid's macroscopic equations, in order to vindicate the approach.

For definiteness we consider the two-dimensional, 9-velocity (D2Q9) LBGK model (figure 1(*A*)) pioneered by Qian *et al* [10] and analysed in detail by Hou *et al* [7]. Denoting vectors of the lattice basis by $\mathbf{c}_i$ (indexing as in figure 1(*A*)), we write collision and subsequent propagation of a generalized D2Q9 LBGK model with a position-dependent scalar collision parameter in the form

$$f_i(\mathbf{r} + \mathbf{c}_i\delta_t, t + \delta_t) = f_i(\mathbf{r}, t) + \frac{1}{\tau(\mathbf{r})}\left(f_i^{(0)} - f_i\right) + F_i. \tag{7}$$

Here the parameter δ_t represents the time step; in the case of constant collision scalar, $\tau(\mathbf{r}) = \tau_0$ determines a *molecular* viscosity

$$\nu_0 = \frac{2\tau_0 - 1}{6}\delta_t \tag{8}$$

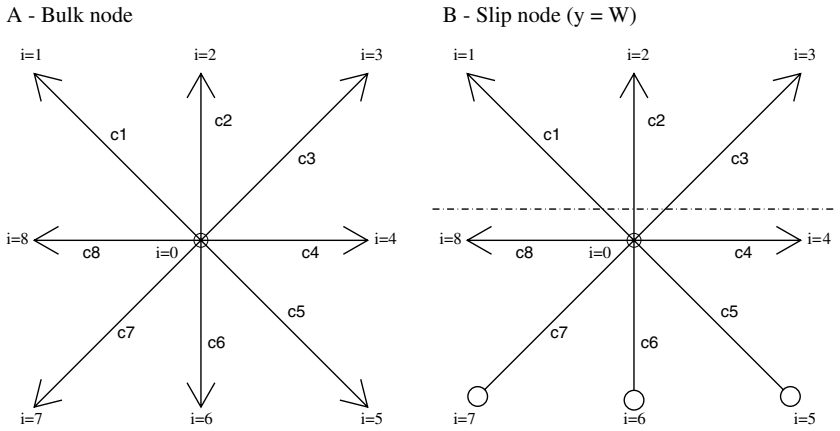

Figure 1. (*A*) Schematic of a bulk node for the D2Q9 lattice. Links are numbered as referred to in the text; link velocity vectors are numbered accordingly. (*B*) Schematic of LB boundary node (top 'wall'), immediately prior to the collision step—propagated data are denoted by arrowheads, unknown link information is denoted by the open circles on links. Here, the (slip) wall location is indicated by the dashed line.

and the additive constant, F_i, represents a *uniform* body force G impressed throughout the lattice fluid [4] according to

$$F_i = 3Gt_p\rho c_{ix} \tag{9}$$

with the constants t_p defined below.

For our model, $\tau(\mathbf{r})$ has spatial dependence which is manipulated to yield an appropriately modified macrodynamic; in particular the usual continuity equation and the *turbulent* Navier–Stokes equations (6) with the coefficient of the dissipative terms modified after equations (3) and (5). In order to maintain the stability of the model, it is further assumed that $0 < 1/\tau(\mathbf{r}) < 2$. As usual, the macroscopic moments for lattice fluid density and momentum are

$$\begin{aligned} \rho &= \sum_i f_i \\ \rho\mathbf{v} &= \sum_i f_i\mathbf{c}_i \end{aligned} \tag{10}$$

and the equilibrium distribution function, $f_i^{(0)}$, is

$$f_i^{(0)}(\rho, \mathbf{v}) = t_p\rho\left[1 + 3\frac{\mathbf{v}\cdot\mathbf{c}_i}{c_s^2} - \frac{3|\mathbf{v}|^2}{2c_s^2} + \frac{9(\mathbf{v}\cdot\mathbf{c}_i)^2}{2c_s^4}\right] \tag{11}$$

where the *weights* $t_p = 4/9, 1/9, 1/36$ for $i = 0, i$ even, i odd, respectively (figure 1(*A*)) and $c_s = 1/\sqrt{3}$ is the velocity of sound, for the D2Q9 lattice. The form of the equilibrium distribution function, (11), ensures that

$$\begin{aligned} \rho &= \sum_i f_i^{(0)} \\ \rho\mathbf{v} &= \sum_i f_i^{(0)}\mathbf{c}_i \end{aligned} \tag{12}$$

and also recovers the non-viscous momentum-flux tensor

$$\Pi_{\alpha\beta}^{(0)} = \sum_i f_i^{(0)} c_{i\alpha}c_{i\beta} = \frac{1}{3}\rho\delta_{\alpha\beta} + \rho v_\alpha v_\beta. \tag{13}$$

Higher-order contributions to the distribution function, $f_i^{(n)}$, introduced through the Chapman–Enskog expansion (e.g., [7])

$$f_i = f_i^{(0)} + \delta_t f_i^{(1)} + \delta_t^2 f_i^{(2)} + \delta_t^3 f_i^{(3)} + \cdots \tag{14}$$

have vanishing first and second moments:

$$\sum_i f_i^{(n)} \Gamma_i = 0 \qquad n > 0 \tag{15}$$

where $\Gamma_i = 1, c_{ix}, c_{iy}$ as a direct consequence of equations (12). However, the second moments of $f_i^{(n)}$ with respect to the lattice basis vectors are not zero.

Travelling the usual road to macrodynamics now: a Taylor expansion of the left-hand side of equation (7); substitution of (14) and of a similarly parametrized time derivative

$$\partial_t = \partial_{t0} + \delta_t \partial_{t1} + \delta_t^2 \partial_{t2} + \delta_t^3 \partial_{t3} + \cdots \tag{16}$$

is followed by a process of collecting terms in powers of the parameter δ_t. We can, thus, write down equations which describe our turbulent LBGK algorithm at order δ_t:

$$(\partial_{t0} + c_{i\alpha}\partial_\alpha) f_i^{(0)} = -\frac{1}{\tau(\mathbf{r})} f_i^{(1)} \tag{17}$$

and at order δ_t^2:

$$\partial_{t1} f_i^{(0)} + (\partial_{t0} + c_{i\alpha}\partial_\alpha)\left(1 - \frac{1}{2\tau(\mathbf{r})}\right) f_i^{(1)} = -\frac{1}{\tau(\mathbf{r})} f_i^{(2)} \tag{18}$$

where the collision parameter, τ, now depends upon the position, $\mathbf{r}$, which is treated as a continuous variable. We do not examine the consequences of expanding τ in powers of the parameter δ_t. By making use of the form of the equilibrium distribution function (11), the result (17) can be used to show to order $\mathbf{u}$ that

$$\sum_i f_i^{(1)} c_{i\alpha} c_{i\beta} = -2c_s^2 \rho \tau(\mathbf{r}) S_{\alpha\beta} \tag{19}$$

where $S_{\alpha\beta}$ is the lattice fluid's rate of strain tensor.

Given the properties of the equilibrium distribution, the modified evolution equation (7) clearly conserves momentum density on the shortest, and hence all, time scales whatever the spatial dependence of $\tau(\mathbf{r})$. One therefore expects to recover an unaltered continuity equation. A detailed analysis of the lattice fluid's continuity equations confirms this; indeed, it is easy to show that position dependence in the collision parameter does not affect either the continuity or Euler equations of the lattice fluid [6] at order δ_t. Accordingly, we proceed directly to the order δ_t^2, Navier–Stokes equations, by making the usual recursive substitution of equation (17) into equation (18):

$$\partial_{t1} f_i^{(0)} + (\partial_{t0} + c_{i\alpha}\partial_\alpha)\left(\tau(\mathbf{r}) - \frac{1}{2}\right)(\partial_{t0} + c_{i\alpha}\partial_\alpha) f_i^{(0)} = -\frac{1}{\tau(\mathbf{r})} f_i^{(2)}. \tag{20}$$

Hence, with variable collision parameter $\tau(\mathbf{r})$ it is possible to obtain, from the first moment of equation (20), a form for the Navier–Stokes equation of the lattice fluid [6]:

$$\partial_t \rho U_\alpha + U_\beta \partial_\beta \rho U_\alpha = -\partial_\alpha P + \partial_\beta \left(\tfrac{1}{6}(2\tau(\mathbf{r}) - 1)\rho S_{\alpha\beta}\right) \tag{21}$$

which is precisely the required form of the turbulent viscosity model, equation (6). Note, however, that the diffusive term of equation (21) contains the lattice fluid's strain rate tensor which can be recovered from equation (19). Note also that the presence of a variable collision parameter in the LB algorithm (7) does not in any way affect the structure of the Navier–Stokes equations when written in the form of equations (1) and (21).

In order to follow Texeira [14], we switch to using $\omega(\mathbf{r}) = 1/\tau(\mathbf{r})$ for collision parameter, with $\omega(\mathbf{r})$ partitioned according to

$$\frac{1}{\omega(\mathbf{r})} = \frac{1}{\omega_0} + \frac{1}{\omega_t(\mathbf{r})} \tag{22}$$

(notation of [14]), in which all the spatial dependence is assumed to reside in the *turbulent* contribution $\omega_t(\mathbf{r})$. Clearly the form of (22) is adapted, on appeal to equations (5), (1) and (21), to allow one to set the molecular viscosity of the lattice fluid independently [14],

$$\nu_0 = \frac{1}{6}\left(\frac{2}{\omega_0} - 1\right) \tag{23}$$

and the turbulent viscosity of the lattice fluid:

$$\nu_t(\mathbf{r}) = \frac{1}{3\omega_t(\mathbf{r})}. \tag{24}$$

In fact, the spatial dependence of the turbulent viscosity (and, thereby, that of the corresponding turbulent contribution to the collision parameter) enters through the contraction $S_{\alpha\beta}S_{\alpha\beta}$ of velocity gradients [16]. To obtain an appropriate form for this turbulent contribution, it is natural to use equation (24) and definition (3). Hence, with the assistance of equation (19) which gives a local identity for $S_{\alpha\beta}$, and from equations (24), (3) and (19) there results an equation for $\omega(\mathbf{r})$ [14]:

$$\frac{1}{3\omega_t(\mathbf{r})} = l_{\mathrm{mix}}^2 \frac{\omega_0\omega(\mathbf{r})}{3\rho(\omega_0 + \omega(\mathbf{r}))} \sum_{ij} \left(f_i - f_i^{(0)}\right)\left(f_j - f_j^{(0)}\right) c_{i\alpha}c_{i\beta}c_{j\alpha}c_{j\beta}. \tag{25}$$

This quadratic may be solved for its positive root:

$$\omega(\mathbf{r}) = \frac{2\omega_0}{1 + \sqrt{\left(1 + 4Q\omega_0^2\right)}} \tag{26}$$

with

$$Q = \frac{9}{2}\frac{l_{\mathrm{mix}}^2}{\rho} \sum_{ij} \left(f_i - f_i^{(0)}\right)\left(f_j - f_j^{(0)}\right) c_{i\alpha}c_{i\beta}c_{j\alpha}c_{j\beta} \tag{27}$$

and where the value of the von Kármán constant K is subsumed in the definition of our choice of l_{mix}.

Here, then, we have an expression for the LBGK collision parameter, which modifies the algorithm to simulate a turbulent fluid, as described by the continuity equation and the mixing-length model of the Reynolds-averaged Navier–Stokes equation. Accordingly we obtain moments of the distribution function which now represent time-averaged quantities.

In the next section, we shall discuss the application of this method to the simulation of internal pressure-driven flow.

3. Turbulent duct flow

In this section, we discuss the application of the LB model described in the last section to simulate internal, pressure-driven, flow in a uniform cross section, infinite aspect ratio duct with smooth walls, over a range of turbulent Reynolds number, Re. In particular, we aim to investigate the turbulent component of the collision parameter, $\omega_t(\mathbf{r})$, the flow profiles and the variation of the friction factor with Re (the Moody curves).

Incompressible, internal, turbulent flow in pipes and ducts is a complicated problem. Different parts of the flow reside in different flow regimes: near the boundary (wall) there

is a narrow but important *viscous sub-layer* in which the velocity varies rapidly, but flow is, for smooth walls at least, laminar [11, 16]. At the centre of the duct, in the so-called *core* flow, there is fully developed turbulence. Between these two regimes there are a number of identifiable interstitials. Correct matching of the sub-layer and the outlying regions to a common *slip* velocity u_s are essential; u_s is usually assumed to be governed by a *law-of-the-wall*. It should be noted that the sub-layer is described by the standard Navier–Stokes equations, and the outlying regions are governed by the Reynolds-averaged Navier–Stokes equations.

The simulations described below take the explicitly modelled boundary to lie parallel with the x-axis, and we impose periodic boundary conditions to form the y-axis boundaries of the flow domain. Clearly the solution must be translationally invariant and, accordingly, flow can be safely induced by a uniform body force [4]. Hence, an additive constant is introduced into the evolution equation (7), since this is the exact equivalent of a uniform pressure gradient in the chosen geometry.

Following traditional CFD [16], we do not attempt explicitly to resolve flow in the laminar viscous sub-layer. Instead, we close the lattice fluid domain by specifying the behaviour of the lattice fluid on the wet face of that sub-layer to be *law-of-the-wall*; i.e. we specify an appropriate *slip* velocity, u_s, for the lattice boundary which also implies an axial rate of strain S_{xy}. The purely axial time-averaged velocity must fall linearly to zero in a sub-lattice distance. Thus, in a practical calculation of pipe flow, a slip velocity u_s is determined via a quantity traditionally denoted by u^* (sometimes called the *stress velocity* [16]), which in turn depends upon the average shear stress on the wall, τ_{wall} [11]:

$$\rho(u^*)^2 = \tau_{\text{wall}} = \frac{(p_1 - p_2)A}{A_{\text{w}}}. \tag{28}$$

Here p_1, p_2 are the pressures at flow stations 1 and 2, assumed to lie a streamwise distance L apart. Also, $A = Wd$ is the cross-sectional area of the duct (W being the duct width and d its (unspecified) depth) and $A_{\text{w}} = 2Ld$ is the area of the wetted perimeter. Accordingly,

$$u^* = \sqrt{\frac{GW}{2\rho}} \tag{29}$$

in which G is the pressure gradient. With a value of u^* given by equation (29), we obtain a slip velocity from the identity (see [16])

$$u_s = u^* \left(\frac{1}{K} \ln y^+ + B \right) \tag{30}$$

in which $K = 0.41$ is the von Kármán constant and B is a constant defined below. $y^+ = yu^*/\nu_0$ is a dimensionless scaling of the distance y in the unmodelled viscous sub-layer. The sub-layer ranges from $y = 0$, at the physical wall, to $y = D$ (to be specified). It is important to note that for the law-of-the-wall to be valid, $0 < y^+(y = D) < 30$. This is achieved by choosing our lattice fluid's molecular viscosity through (8), and its stress velocity by appropriate choice of the pressure gradient and duct width in equation (29).

For our LB simulations, we choose $D = 0.99$ lattice units. The corresponding velocity gradients at the unmodelled (off lattice) boundary now follow from the slip velocity (30) and the assumed depth D of the viscous sub-layer:

$$S_{xy} = S_{yx} = \pm\frac{u^*}{D} \qquad S_{xx} = S_{yy} = 0. \tag{31}$$

Thus, the lattice fluid's domain is effectively bounded by a sub-lattice viscous sub-layer of specified depth D, the inner edge of which moves with a slip velocity consistent with the

law-of-the-wall, and which ensures the correct average shear stress at the unmodelled (physical) wall.

In [5], we developed a method for closing an LB simulation lattice with verifiably correct hydrodynamic behaviour, i.e. of setting densities, f_i, on the undefined links with values consistent with those populating bulk lattice node at the lattice edge. The particular lattice basis considered there was D2Q9 and the Dirichlet boundaries were taken to be planar. The explicitly modelled boundaries of our duct are themselves planar and so the closure strategy developed in [5] may be used directly. Figure 1(*B*) depicts a 'law-of-the-wall' node, terminating our D2Q9 lattice at the $y = W - D$ modelled wall. The dotted line shows the supposed location of the slip boundary. Clearly links $i = 1, 2, 3$ are 'cut', the remaining links being taken to lie within the simulation domain, precisely at the edge of the viscous sub-layer. Accordingly a post-propagation value of f_i exists for all boundary nodes' links *except* those characterized by $i = 5, 6, 7$ (indicated by the use of circles as opposed to arrows in figure 1(*B*)). Using the method of [5], we can construct second-order correct f_i for these links, chosen to recover the target slip velocity at the boundary and the corresponding stress. The latter quantity is calculated directly from the region of the boundary, using finite differences.

4. Results: flow profiles and Moody curve

In this section we discuss results for turbulent duct flow. Throughout, $\bar{v}$ denotes the cross-duct average velocity, W the physical width of the duct and ν_0 is the *molecular* viscosity of the lattice fluid. The fluid is forced parallel to the x-direction by the application of a uniform body force, $F_i = 3Gt_p\rho c_{ix}$. The forcing must be small to maintain stability when the lattice fluid has the small viscosity necessary to access the large Reynolds numbers which, in many applications, characterize turbulent duct flow. Accordingly, for all the results presented here, $G = 1.5 \times 10^{-5}$ was chosen alongside a lattice y-dimension of 60 lattice units. The simulations correspond to constant spatial resolution. Also, the physical width of the simulated duct is actually $60 + 2D$, where D is the width of the sub-layer. The initial density of the lattice fluid was chosen to be 1.8, the von Kármán constant was chosen to be $K = 0.41$ and the constant B which appears in our form of the law-of-the-wall was chosen to be 5.0, a value consistent with smooth walls [16].

In order to ensure sufficiently large Reynolds numbers

$$Re = \frac{2W\bar{v}}{\nu_0} \tag{32}$$

consistent with turbulent duct flow, the molecular component of the collision parameter was varied in a range $1.991 < \omega_0 < 1.999$, close to its maximum value of 2 (where the corresponding variation in the molecular viscosity is rapid). The resulting variation in the measured Reynolds number was found to be $10^4 < Re < 10^5$: well into the turbulent regime. The convergence of the data was slow (several tens of thousands of time steps) on account of the very small molecular viscosities in use. All the data presented derive from steady-state velocity fields which have evolved for many thousands of time steps, without fluctuation.

Figure 2 shows the variation in the steady-state velocity profile with y distance across the duct, measured after 7×10^5 time steps, for $\omega_0 = 1.995$, resulting in an average velocity (calculated by use of the trapezium rule and corrected for the viscous sub-layer) of $\bar{v} = 0.069\,722$, yielding $Re = 20\,357$. The velocity profile shown in figure 2 into which the unmodelled sub-layer data have been inserted, clearly exhibits all the expected characteristics of a turbulent profile [11, 16], across the whole width of the duct, without any spurious slip velocities at the boundary, either at the wet boundary of the viscous sub-layer or at the wall.

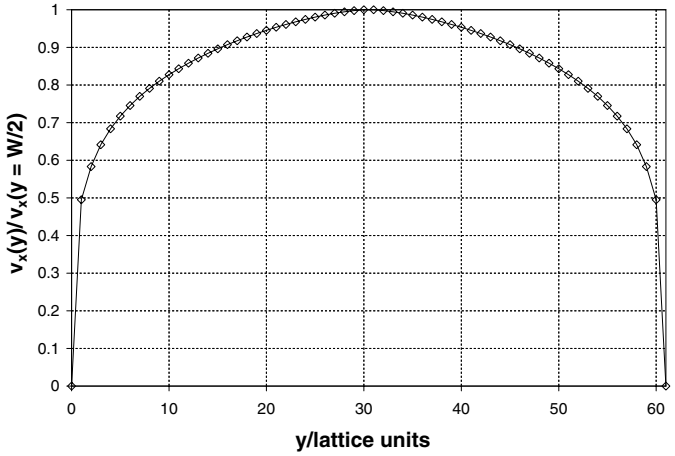

Figure 2. Steady-state velocity profile, measured after 7×10^5 time steps, for $\omega_0 = 1.995$, resulting in an average velocity (calculated by use of the trapezium rule and corrected for the viscous sub-layer) of $\bar{v} = 0.069\,722$, yielding $Re = 20\,357$.

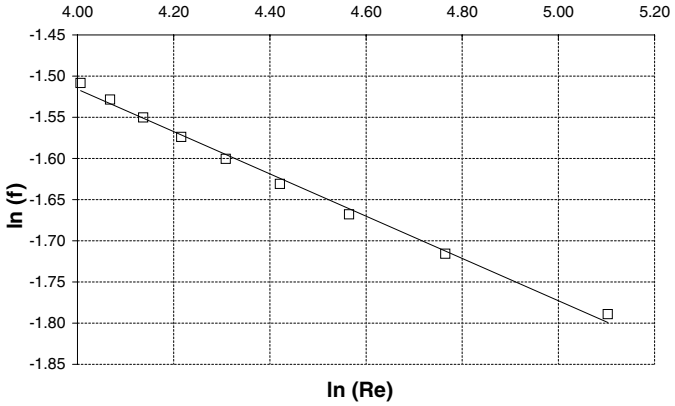

Figure 3. Moody curve from the simulation data: the (logarithmic) variation of measured Darcy–Weisbach friction factor, f, for Reynolds number Re in the range $10^4 < Re < 10^5$.

A much more stringent test of the model (core and boundary algorithm together) resides in its ability to correctly recover stresses at the duct wall, which may be assessed by considering the Darcy–Weisbach friction factor

$$f = \frac{GW}{\frac{1}{2}\rho\bar{v}^2} \tag{33}$$

where G, the pressure gradient, was set as discussed above. The friction factor was measured directly and figure 3 shows its (logarithmic) variation over the range of Reynolds number specified above. This branch of the Moody curves of course corresponds to smooth duct walls (reflected in our choice of $B = 5.0$ in equation (30)). However, wall roughness was also successfully modelled in the traditional way, by changing the value of the constant B. The data of figure 3 are in excellent agreement with the experimental data [9].

Figure 4 shows a typical variation with cross-duct distance y of the full and turbulent component, ω and ω_t, respectively, of the LB collision parameter. The variation in the

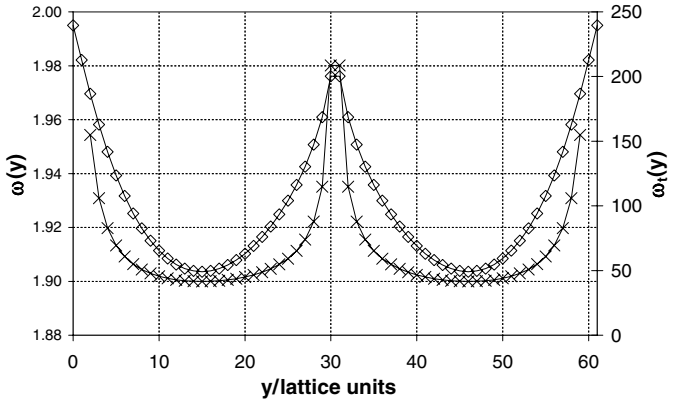

Figure 4. Left axis (diamonds): a typical variation in the overall collision parameter ω with cross-duct distance y. This variation is notably small, as one might expect considering that values of ω close to 2.0 accommodate a large range of kinematic viscosities. Right axis (crosses): corresponding variation in the turbulent component ω_t of the LB collision parameter. Simulation data correspond to that characterizing figure 2.

effective value of ω is notably small, as one might expect, considering that values of ω close to 2.0 accommodate a large range of kinematic viscosities. The simulation data and Reynolds number are as in figure 2.

5. Conclusions and future work

Possibly the most interesting theoretical point we would like to make, arises from the treatment, in section 2, of Teixeira's method [14] of 'turbulent modification' to the basic LB algorithm, through what is essentially a shear-dependent relaxation parameter. This shows that the Chapman–Enskog derivation of the macrodynamics of an LB model (the traditional way of deriving the model's dynamics) exactly yields the (time-averaged) influence of turbulence as additional, modelled stresses. This precise correspondence, with a form of the Reynolds-averaged Navier-Stokes equations, without additional error, is not necessarily accidental and may be regarded as a consequence of the essential LB algorithm: the momentum densities interact in this (and most other LB) schemes at a point, i.e. through a 'zero-ranged' potential. Mathematically, the position of the viscosity terms on the right-hand side of the Navier–Stokes equation (in the 'right' position, sandwiched between differential operators) arises out of the structure of the Chapman–Enskog derivation of the dynamics, in which time scales associated with particular processes are effectively separated, which may also be significant.

In practical terms, we have implemented a method, after Teixeira, for simulating turbulent flow, using a lattice Boltzmann simulation adapted to the Prandtl mixing-length model of the Reynolds-averaged Navier–Stokes equations. The method has been validated for internal, incompressible flow in an infinite aspect ratio duct. The method relies upon the imposition of a second-order accurate boundary strategy to enable law-of-the-wall closure of the simulation lattice. The stringent test of Reynolds number variation of Darcy–Weisbach friction factor (equation (33)), shown in figure 3, decisively supports the observation that our implementation is capable of representing smooth-walled duct flow. Moreover, results for walls of variable roughness can be recovered from our model straightforwardly, using the usual device of varying the law-of-the-wall parameter B, equation (30).

Of course, in applications, cylindrical pipe flow is far more common than duct flow. The method presented here could be adapted, to the simulation of cylindrical pipe flow, using the method [4] of expressing a lattice Boltzmann fluid flow problem with axial symmetry in a one coordinate system. The encouraging nature of the results recovered from this rather simpler problem certainly indicate that to do so would be a worthwhile undertaking, especially as there is a larger body of data for this type of turbulent flow [17].

References

[1] Care C M, Halliday I and Good K 2000 *J. Phys.: Condens. Matter* **12** L665
[2] www.exa.com
[3] Filippova O, Succi S, Mazzacco F, Arrighetti C, Bella G and Hanel D 2001 *J. Comp. Phys.* **170** 812
[4] Halliday I, Hammond L A, Care C M, Good K and Stevens A 2001 *Phys. Rev.* E **64** 011208
[5] Halliday I, Hammond L A and Care C M 2002 *J. Phys. A: Math. Gen.* **35** L157
[6] Hammond L A 2002 *PhD Thesis* Sheffield Hallam University
[7] Hou S, Zou Q, Chen S, Doolen G D and Cogley A C 1995 *J. Stat. Phys.* **118** 329
[8] Koponen A, Kataja M, Timonen J and Kandhai D 1998 *Int. J. Mod. Phys.* C **9** 1505
[9] Nikuradse J 1932 *V.D.I. Forschungsheft* 356
[10] Qian Y H, d'Humières D and Lallemand P 1992 *Europhys. Lett.* **17** 479
[11] Reynolds A J 1972 *Turbulent Flows in Engineering* (New York: Wiley)
[12] Succi S 2001 *The Lattice Boltzmann Equation* (Oxford, UK: Clarendon Press)
[13] Swift M R, Orlandini E, Osborn W R and Yeomans J M 1996 *Phys. Rev.* E **54** 5041
[14] Teixeira C M 1998 *Int. J. Mod. Phys.* C **9** 1159
[15] Thomson S P, Halliday I and Care C M 1999 *Phys. Chem. Chem. Phys.* **1** 2183
[16] Versteeg H K and Malalasekera W 1995 *An Introduction to Computational Fluid Dynamics* (Englewood Cliffs, NJ: Prentice Hall)
[17] Zagarola M V 1996 *PhD Thesis* Princeton University